# AUTO-TUNING OF PRECISION SERVO CONTROLLERS SUFFERING FROM LARGE MASS RATIO INDUCED VIBRATIONS

Alper Dumanli<sup>1</sup>, Jeff Lowe<sup>2</sup>, Sinan Badrawy<sup>2</sup>, Burak Sencer<sup>1</sup>

<sup>1</sup>School of Mechanical, Industrial and Manufacturing Engineering

Oregon State University

Corvallis, Oregon, USA

<sup>2</sup>Moore Nanotechnology Systems

Swanzey, New Hampshire, USA

#### INTRODUCTION

This paper presents an automated controller tuning strategy for precision servo positioning systems suffering from large inertial load ratio induced vibrations. Typical industrial ultaprecision feed drive systems are designed based on direct driven linear motor systems and controlled by PID controllers tuned based on nominal inertia. When large loads are attached on the feed drive, robustness of the PID controller may not suffice, and feedback control loop may suffer from unwanted vibrations [1]. This vibratory behavior originates mainly from shrinking stability margins of the servo control system and potentially causes instability [2]. Moreover, varying load inertia hinders accuracy of feedforward (FF) compensators, which are typically designed based on the inverse of the nominal system [3]. This paper considers dynamics of ultra-precision feed drive systems and presents an auto-tuning algorithm to stabilize feedback controllers considering attached load inertia. The auto-tuning strategy is based on on-machine measured frequency response function (FRF). The PID controller is augmented with a simple feedback filter whose parameters are automatically tuned to attain desired phase and gain margins. In addition, a trajectory pre-filter is designed and iteratively tuned to further improve the tracking performance. Effectiveness of the proposed strategy is verified on an actual ultra-precision machine tool (Nanotech 650FG-v<sup>2</sup> freeform generator) shown in Fig. 1.a.

Overall block diagram of the proposed strategy is given in Fig. 2. Proposed control system consists of three key components: (1) a PID controller K(z) to meet cross-over frequency and phase margin requirements, (2) a low pass filter H(z) to suppress higher order dynamics and ensure stability, and finally (3) a Trajectory Pre-

Filter P(z) to modify the reference trajectory in order to increase tracking bandwidth.

# MODELING OF PRECISION SERVO MECHANISMS WITH LARGE LOAD INERTIA

In typical industrial applications, servo-drives are modeled as a rigid body with a moment of inertia of  $J_D$  [kgm<sup>2</sup>]. With a load/workpiece attached, the overall model of the system becomes:

$$\frac{\theta}{\tau} = G = \frac{1}{\left(J_D + J_L\right)s^2 + bs} \tag{1}$$

where G is the rigid body transfer function (TF).  $\theta$  and  $\tau$  are the measured angular displacement and motor torque input.  $J_L$  is the inertia of the load (workpiece), and b is the equivalent viscous friction coefficient.

a) Experimental setup with large load inertia

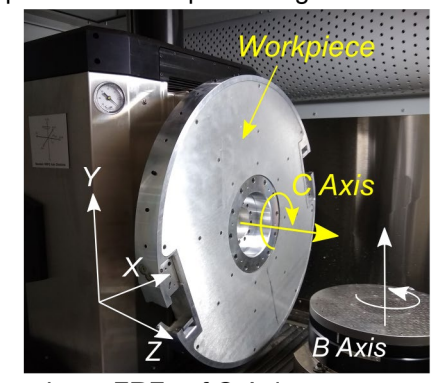


FIGURE 1: Experimental setup (a) and FRFs(b).

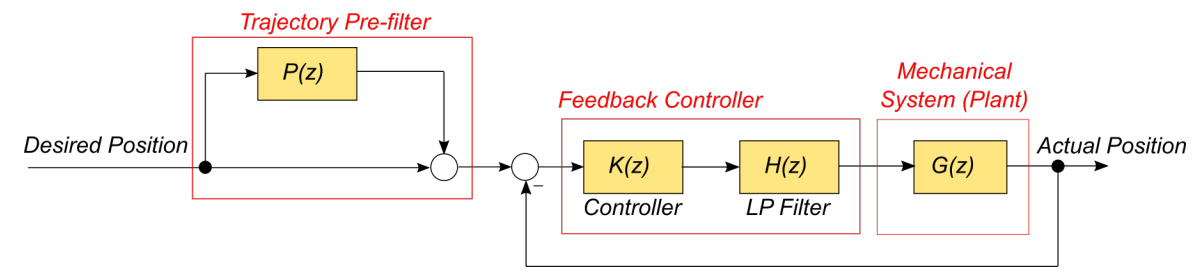


FIGURE 2: Block diagram of the proposed control scheme.

This model captures the system dynamics for typical applications. However, if the load inertia  $J_L$  increases excessively, i.e.  $J_L >> J_D$ , higher order dynamics invalidates the modeling accuracy of G, and measured and modeled FRFs differ significantly (see Fig. 1.b). Thus, closed loop controllers designed by using G may not provide robust stability. In order to retain stability of the servo-loop, a PID controller is designed based on G, and the controller is augmented by a low-pass filter designed considering the measured FRF of the servo positioning system  $G_{FRF}$ . Design of these two components are described in the following.

## **CLOSED LOOP CONTROLLER DESIGN**

The closed loop PID controller is designed in order to ensure that the loop transmission TF, L=KG, has the desired cross-over frequency and phase margin, where K is defined in discrete frequency-domain as:

$$K(z) = K_p \left(1 + K_I \left(\frac{T_s z}{z - 1}\right)\right) + K_D \left(\frac{z - 1}{T_s z}\right)$$
 (2)

with  $K_P$ ,  $K_I$  and  $K_P$  being the PID controller gains. and z is the discrete frequency (z-Transform) variable. The acceptable value of the cross-over frequency is determined by examining the discrepancy between modeled measured ( $G_{FRF}$ ) FRFs. First, the smallest frequency at which  $G_{FRF}$  deviates from G more than +3[dB] is determined. This frequency is denoted as  $\omega_{lim}$ . Next, to ensure robust avoidance of modeling mismatches, cross-over frequency ( $\omega_c$ ) is selected as:  $\omega_c$ =0.2 $\omega_{im}$ . On the experimental setup shown in Fig 1.a, this corresponds to  $\omega_{lm}$ =115[Hz] and  $\omega_c$ =23[Hz]. This quarantees that the controller only acts on the portion of the system with significantly high modeling accuracy. The phase-margin is selected as 65[deg], which is typical for industrial applications. The PID gains are determined to meet the cross-over frequency and phase margin requirements as described in the following.

First, the integral gain is calculated as  $K_I$ =0.1 $\omega_c$  to ensure that the phase lag introduced by numerical integration does not influence the loop phase in the vicinity of  $\omega_c$ . Next,  $K_P$  and  $K_D$  gains are determined to meet the cross-over frequency ( $\omega_c$ ) and phase margin (PM) requirements given by:

$$L_{Re} = K_{Re}G_{Re} - K_{Im}G_{Im} = \cos(180^{\circ} + PM)$$

$$L_{Im} = K_{Re}G_{Im} + K_{Im}G_{Re} = \sin(180^{\circ} + PM)$$
(3)

where  $L_{Re}=Re\{L(e^{j\omega cTs})\}$  and  $L_{Im}=Im\{L(e^{j\omega cTs})\}$ . Notice that Eq. (3) poses a simple linear system of equations, and  $K_P$  and  $K_D$  can be obtained as:

$$\begin{bmatrix} K_{P} \\ K_{D} \end{bmatrix} = \Omega^{-1} \begin{bmatrix} \cos(180^{\circ} + PM) \\ \sin(180^{\circ} + PM) \end{bmatrix}, \text{ where:}$$

$$\Omega = \begin{bmatrix} K_{Re}^{(1)}G_{Re} - K_{lm}^{(1)}G_{lm} & K_{Re}^{(2)}G_{Re} - K_{lm}^{(2)}G_{lm} \\ K_{Re}^{(1)}G_{lm} + K_{lm}^{(1)}G_{Re} & K_{Re}^{(2)}G_{lm} + K_{lm}^{(2)}G_{Re} \end{bmatrix}$$

$$K^{(1)} = 1 + \frac{\omega_{c}}{10} \left( \frac{T_{s}e^{j\omega_{c}T_{s}}}{e^{j\omega_{c}T_{s}} - 1} \right), K^{(2)} = \frac{e^{j\omega_{c}T_{s}} - 1}{T_{s}e^{j\omega_{c}T_{s}}}$$

$$(4)$$

where  $T_s$  is the sampling period. The designed PID controller is implemented utilizing the Delta-Tau servo-driver on board with the ultra-precision machine tool. Modeled (L) and measured ( $L_{FRF}$ ) loop transmission FRFs are shown in Fig. 3.

As seen, desired crossover frequency and phase margin are achieved. At high frequencies, i.e.  $\omega > \omega_{lim}$ ,  $L_{FRF}$  deviates from L significantly, and instability occurs at ~1.2[kHz] with a -8.64[dB] gain margin. In order to mitigate this model-measurement deviation and retain closed loop stability, an optimal low pass filter design strategy is proposed in the following section.

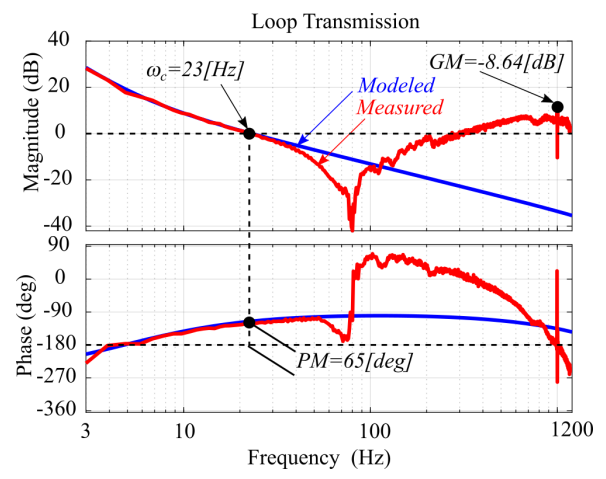


FIGURE 3: Loop transmission FRFs with PID controller. Note that PID controller by itself cannot prevent high frequency instability.

#### **OPTIMAL LOW PASS FILTER DESIGN**

This section describes the low pass filter design procedure in order to eliminate closed loop stability issues caused by modelling inaccuracies. Low pass filter *H* (see Fig. 2) is designed in continuous Laplace (s) domain as:

$$H(s) = \frac{1}{c_2 s^2 + c_1 s + c_0}$$
 (5)

where  $c_0...c_2$  are the design parameters. The low pass filter is then converted into discrete (z) domain for implementation. The purpose of H is to ensure that loop transmission magnitude do not increase after the desired crossover frequency is achieved. This objective is expressed as an optimization problem as:

$$\min_{H(s)} \left| L\left(e^{j\omega T_{s}}\right) H\left(j\omega\right) - L\left(e^{j\omega T_{s}}\right) \right| \\
\text{subject to:} \\
\left| L_{FRF}\left(e^{j\omega T_{s}}\right) H\left(j\omega\right) \right| \leq \alpha, \text{ for } \omega \geq \omega_{\lim} \\
H(s) \text{ is stable.}$$
(6)

where  $\alpha$  is the maximum allowable loop transmission magnitude for frequencies higher than  $\omega_{lim}$ . Notice that the magnitude operator, i.e. |.|, is used in both the objective function and the inequality constraints of Eq. (6). This nonlinearity causes the optimization problem to be nonconvex, and thus the solution suffers from local minima, numerical inefficiency and inaccuracy. To circumvent this, Eq. (6) is modified to pose a convex optimization problem. This is done by substituting the magnitude operator by the two norm,  $||.||_2$ , acting on the real and imaginary parts of the TFs. Additionally, H is

substituted by  $H^{-1}$  to ensure that the decision variables  $c_0...c_2$  appear linearly in the optimization objective and constraints. The modified optimization problem is written as:

$$\min_{\boldsymbol{H}^{-1}(s)} \left( \left\| \operatorname{Re}\left\{ L\left(\mathbf{e}^{j\omega T_{s}}\right) \boldsymbol{H}^{-1}\left(j\omega\right) - L\left(\mathbf{e}^{j\omega T_{s}}\right) \right\} \right\|_{2}^{2} \cdots + \left\| \operatorname{Im}\left\{ L\left(\mathbf{e}^{j\omega T_{s}}\right) \boldsymbol{H}^{-1}\left(j\omega\right) - L\left(\mathbf{e}^{j\omega T_{s}}\right) \right\} \right\|_{2}^{2} \right)$$

subject to:

$$|\operatorname{Re}\left\{H^{-1}(j\omega)\right\} \leq -\left|\operatorname{Re}\left\{L_{FRF}\left(\mathbf{e}^{j\omega T_{s}}\right)\right\}\right| \frac{1}{\alpha}$$

$$|\operatorname{Im}\left\{H^{-1}(j\omega)\right\} \geq \left|\operatorname{Im}\left\{L_{FRF}\left(\mathbf{e}^{j\omega T_{s}}\right)\right\}\right| \frac{1}{\alpha}$$
for  $\omega \geq \omega_{\lim}$ 

H(s) is stable.

Notice that Eq. (7) minimizes real and imaginary parts of (L(z)H(s)-L(z))/H(s), instead of the magnitude of L(z)H(s)-L(z) as in Eq. (6). Since H(s) has small magnitude at high frequencies (imposed by inequality constraints), division by H(s) does not change the objective function significantly. Conversion of the inequality constraints from Eq. (6) to Eq. (7) follows from:

$$\left| L_{FRF} \left( \mathbf{e}^{j\omega T_{s}} \right) H(j\omega) \right| \leq \alpha \rightarrow \left| H^{-1} \left( j\omega \right) \right| \geq \frac{1}{\alpha} \left| L_{FRF} \left( \mathbf{e}^{j\omega T_{s}} \right) \right|$$

$$\operatorname{Re} \left\{ H^{-1} \left( j\omega \right) \right\}^{2} + \operatorname{Im} \left\{ H^{-1} \left( j\omega \right) \right\}^{2} \geq \cdots$$

$$\frac{1}{\alpha^{2}} \left( \operatorname{Re} \left\{ L \left( j\omega \right) \right\}^{2} + \operatorname{Im} \left\{ L \left( j\omega \right) \right\}^{2} \right)$$
(8)

$$\operatorname{Re}\left\{H^{-1}(j\omega)\right\}^{2} \ge \frac{1}{\alpha^{2}}\operatorname{Re}\left\{L(j\omega)\right\}^{2}$$

$$\operatorname{Im}\left\{H^{-1}(j\omega)\right\}^{2} \ge \frac{1}{\alpha^{2}}\operatorname{Im}\left\{L(j\omega)\right\}^{2}$$
(9)

Eq. (8) is derived from the inequality constraint of Eq. (6). Taking the square root of both sides of Eq. (9) gives the inequality constraints in Eq. (7). Notice that in Eq. (7), real part of the inequality constraints is imposed to be negative, and the imaginary part is imposed to be positive. This enforces H(s) to have a phase angle within the interval [-90°, -180°] for  $\omega > \omega_{lim}$ , and guarantees that the filter suppresses the magnitude of its input in this frequency region. Eq. (7) poses a linear least squares minimization problem with linear inequality constraints. It is convex and can be solved to global optimality efficiently. Finally, it is put in matrix-vector form to obtain the parameters of H,  $(c_0...c_2)$ , as shown in Eq. (10) at the top of the next page. Notice that the inequality constraint x≥0 in Eq. (10) ensures stability of H(s), and the equality constraint  $c_0$ =1 imposes unity gain at "zero" frequency, and therefore the low pass filter does not introduce additional gain to the loop.

$$\min_{c_0, c_1, c_2} \|\mathbf{A}\mathbf{x} - \mathbf{b}\|_2^2$$
subject to:  $\mathbf{C}\mathbf{x} \le \mathbf{d}$ ,  $\mathbf{x} \ge 0$  and  $c_0 = 1$ 

where:  $\mathbf{x} = \begin{bmatrix} c_2 & c_1 & c_0 \end{bmatrix}$ 

$$= \begin{bmatrix} -\omega_1^2 \operatorname{Re}\left\{L\left(e^{j\omega_1 T_s}\right)\right\} & -\omega_1 \operatorname{Im}\left\{L\left(e^{j\omega_1 T_s}\right)\right\} & 1 \\ \vdots & \vdots & \vdots \\ -\omega_N^2 \operatorname{Re}\left\{L\left(e^{j\omega_1 T_s}\right)\right\} & -\omega_N \operatorname{Im}\left\{L\left(e^{j\omega_1 T_s}\right)\right\} & 1 \\ -\omega_1^2 \operatorname{Im}\left\{L\left(e^{j\omega_1 T_s}\right)\right\} & \omega_1 \operatorname{Re}\left\{L\left(e^{j\omega_1 T_s}\right)\right\} & 0 \\ \vdots & \vdots & \vdots \\ -\omega_N^2 \operatorname{Im}\left\{L\left(e^{j\omega_1 T_s}\right)\right\} & \omega_N \operatorname{Re}\left\{L\left(e^{j\omega_N T_s}\right)\right\} & 0 \end{bmatrix}$$

$$= \begin{bmatrix} \operatorname{Re}\left\{L\left(e^{j\omega_1 T_s}\right)\right\} \\ \vdots \\ \operatorname{Im}\left\{L\left(e^{j\omega_1 T_s}\right)\right\} \\ \vdots \\ \operatorname{Im}\left\{L\left(e^{j\omega_1 T_s}\right)\right\} \end{bmatrix} \\ \vdots \\ \operatorname{Im}\left\{L\left(e^{j\omega_1 T_s}\right)\right\} \end{bmatrix} \\ \vdots \\ -\left|\operatorname{Re}\left\{L_{FRF}\left(e^{j\omega_1 T_s}\right)\right\}\right| \\ \vdots \\ -\left|\operatorname{Im}\left\{L_{FRF}\left(e^{j\omega_1 T_s}\right)\right\}\right| \\ \vdots \\ -\left|\operatorname{Im}\left\{L_{FRF}\left(e^{j\omega_1 T_s}\right)\right\}\right| \\ \vdots \\ -\left|\operatorname{Im}\left\{L_{FRF}\left(e^{j\omega_1 T_s}\right)\right\}\right| \\ \vdots \\ = \left|\operatorname{Im}\left\{L_{FRF}\left(e^{j\omega_1 T_s}\right\}\right| \\ = \left|\operatorname{Im}\left\{L_{FRF}\left(e^{j\omega_1 T_s}\right)\right\}\right| \\ = \left|\operatorname$$

Once H(s) is designed in continuous domain, it is discretized (H(z)) and implemented in the control loop as shown in Fig 2. Comparison of loop transmission performance with and without H is given by Fig 4. As seen, the low pass filter H suppresses higher order dynamics at high frequencies and retains closed loop stability without altering frequency domain design specifications (crossover frequency and phase margin).

# TRAJECTORY PRE-FILTER DESIGN

The closed loop controller designed in the previous section provides a command tracking bandwidth  $(\omega_{BW})$  close to the crossover frequency  $\omega_{BW}\cong\omega_c$ . In high-speed industrial applications, reference trajectories contain rapidly varying acceleration/deceleration

segments, and thus they may have frequency components in their spectra that are beyond  $\omega_{\rm c}$ . As a result; inertial forces, low pass filter dynamics and high frequency modeling errors may cause large tracking errors due to insufficient tracking bandwidth. To increase the tracking bandwidth, a trajectory pre-filter P is proposed as shown in Fig. 2.

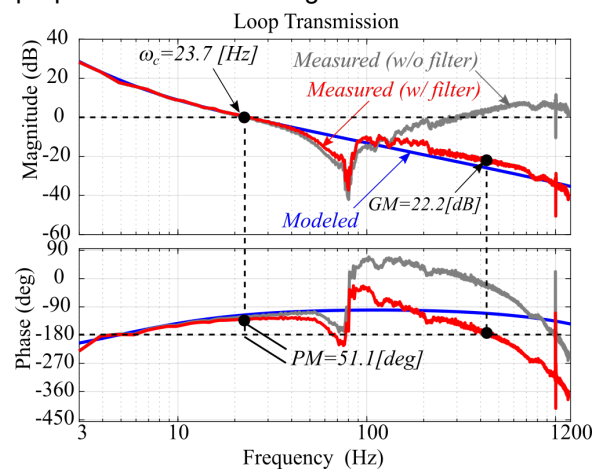


FIGURE 4: Comparison of loop transmission FRFs with and without the optimally designed low pass filter.

The filter structure is selected in order to achieve near-perfect tracking as:

$$\frac{\theta}{\theta_{P}} = (1+P)\frac{KHG}{1+KHG} \cong 1 \rightarrow P = \frac{1}{KHG}$$
 (11)

where  $\theta_R$  is the reference angular displacement command. K and H are known by design. However, mismatch between G and  $G_{FRF}$  may lead to a sub-optimal implementation of P as given in Eq. (11). To ensure that P is designed optimally, its parameters are identified iteratively through on-site measured data as described in the following.

First, P is optimized by assuming K and G dominate the closed loop dynamics. This assumption is valid for lower frequencies, since H starts influencing loop transmission TF for frequencies higher than  $\omega_{lim}$ . By assuming H=1, tracking error (e= $\theta_R$ - $\theta)$  dynamics in continuous frequency and time domains are written as:

$$\frac{e}{\theta_{R}} = \frac{Js^{3} + bs^{2}}{Js^{3} + (K_{D} + b)s^{2} + K_{P}s + K_{P}K_{I}}$$

$$\ddot{e} = \ddot{\theta}_{R} - \frac{1}{J} \left( (K_{D} + b)\dot{e} + K_{P}e + K_{P}K_{I} \int_{0}^{t} ed\tau - b\dot{\theta}_{R} \right)$$
(12)

where  $J=J_D+J_L$ . Notice that Eq. (12) contains critical parameters that are useful for identifying P such as J and b. Controller parameters  $K_P$ ,  $K_D$ 

and  $K_l$  are already known by design. However, J and b may not be accurately identified through frequency domain-based (FRF) identification. To circumvent this, J and b values are estimated through a simple back-and-forth trajectory tracking experiment. The position data recorded by this experiment is utilized to form the following optimization problem derived by Eq. (12):

 $\min_{J_e,b_e} \|\Phi \Lambda - \Psi\|_2^2$ , subject to:  $J_e \ge 0$  and  $b_e \ge 0$ 

$$\Phi = \begin{bmatrix}
\ddot{e}(0) & \dot{e}(0) & e_{i}(0) & -\dot{\theta}_{R}(0) \\
\ddot{e}(T_{s}) & \dot{e}(T_{s}) & e_{i}(T_{s}) & -\dot{\theta}_{R}(T_{s}) \\
\vdots & \vdots & \vdots & \vdots \\
\ddot{e}(MT_{s}) & \dot{e}(MT_{s}) & e_{i}(MT_{s}) & -\dot{\theta}_{R}(MT_{s})
\end{bmatrix} (13)$$

$$\Psi = \begin{bmatrix}
\ddot{\theta}_{R}(0) - e(0) \\
\ddot{\theta}_{R}(T_{s}) - e(T_{s}) \\
\vdots \\
\ddot{\theta}_{R}(MT_{s}) - e(MT_{s})
\end{bmatrix}, \Lambda = \begin{bmatrix}
K_{D} + b \\
K_{P} \\
K_{P}K_{I} \\
b
\end{bmatrix}$$

where M is the number of samples for the trajectory following experiment, and  $e_i$  is the numerically integrated error signal.  $J_e$  and  $b_e$  are the estimated inertia and viscous friction coefficient. Notice that Eq. (13) is a convex optimization problem, and thus its globally optimal solution can be obtained efficiently. Once Eq. (13) is solved, the "rough" pre-filter  $P_1$  (without including H) is implemented in discrete domain as:

$$P_{1} = \frac{J_{e} \left(\frac{z-1}{T_{s}z}\right)^{2} + b_{e} \left(\frac{z-1}{T_{s}z}\right)}{K_{P} \left(1 + K_{I} \left(\frac{T_{s}z}{z-1}\right)\right) + K_{D} \left(\frac{z-1}{T_{s}z}\right)}$$
(14)

By implementing this trajectory pre-filter, tracking performance can be increased greatly. Fig. 5 shows an example trajectory following experiment with a total displacement of 2 [deg]. Maximum velocity and acceleration of the reference trajectory are selected as 5 [deg/sec] and 50 [deg/sec²]. As seen, tracking error peaks reach up to 4 [mdeg] without the pre-filter. With the pre-filtered trajectory, maximum tracking error peak is reduced to  $\sim$ 570 [µdeg].

Although the error reduction shown in Fig. 5 is significant, there are still some residual error peaks when  $P_1$  is used. These errors are attributed to the phase lag introduced by the low pass filter and power electronics circuitry as well as high frequency dynamics of the mechanical system. In order to eliminate these remaining errors, the pre-filter structure is augmented by

second order finite impulse response filter (FIR) dynamics as:

$$P = P_1 (n_0 + n_1 z^{-1} + n_2 z^{-2})$$
 (15)

The new set of parameters for  $P(n_0...n_2)$  are identified through machine-in-the-loop optimization, by minimizing the trajectory tracking errors as:

$$\min_{n_0, n_1, n_2} \left( J_{\text{Cost}} = \frac{1}{2} \| \mathbf{e} \|_2^2 \right)$$
 (16)

where  ${\bf e}$  is the vector of tracking error data obtained by the tracking experiment shown in Fig. 5.

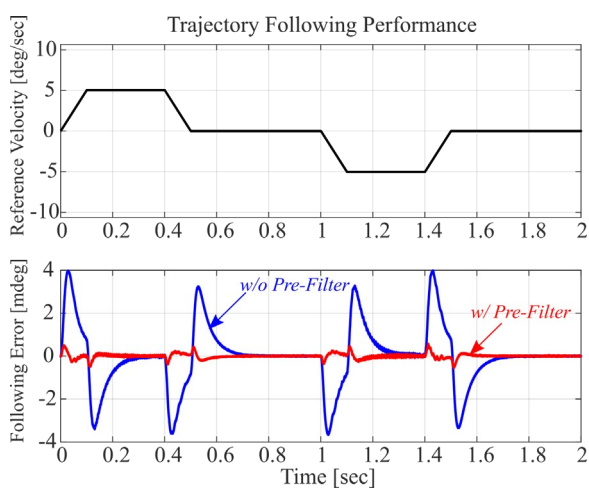


FIGURE 5: Trajectory tracking performance with and without "rough" pre-filter.

Eq. (16) is a convex optimization problem, and thus utilizing the gradient  $\nabla J_{Cost}$  and Hessian  $\nabla^2 J_{Cost}$  of its cost function enables us to rapidly and safely guide the parameter search to global optimum. Note that,  $\mathbf{e}$  is already available from the trajectory following experiment, and its gradient  $\nabla \mathbf{e}$  is obtained as:

$$\mathbf{e} = \left(\frac{1 - PG_{FRF}KH}{1 + G_{FRF}KH}\right)\theta_{R}$$

$$\nabla \mathbf{e} = \begin{bmatrix} \frac{\partial \mathbf{e}}{\partial n_{0}} \\ \frac{\partial \mathbf{e}}{\partial n_{1}} \\ \frac{\partial \mathbf{e}}{\partial n_{2}} \end{bmatrix} = -\nabla P\underbrace{\left(\frac{G_{FRF}KH}{1 + G_{FRF}KH}\right)\theta_{R}}_{\theta} \qquad (17)$$

$$\nabla P = -\begin{bmatrix} 1 \\ \mathbf{z}^{-1} \\ \mathbf{z}^{-2} \end{bmatrix} P_{1}$$

Notice that the actual angular displacement  $(\theta)$  appears in Eq. (17), which is obtained experimentally. Therefore, the error gradient  $\nabla \mathbf{e}$  can be calculated in a complete data-driven fashion, without requiring any system model. The calculated gradient is then used to guide the machine-in-the-loop parameter search using Newton's second order iteration scheme as:

$$\begin{bmatrix} n_0 \\ n_1 \\ n_2 \end{bmatrix}^{k+1} = \begin{bmatrix} n_0 \\ n_1 \\ n_2 \end{bmatrix}^k - \eta \left( \nabla \mathbf{e}^T \nabla \mathbf{e} \right)^{-1} \left( \mathbf{e}^T \nabla \mathbf{e} \right) \quad (18)$$

where  $\eta$  is the learning rate. It can be shown that  $0 \le \eta \le 1$  guarantees monotonic convergence to global optimum [4], and  $\eta$  is selected as 1.

Fig. 6.a shows trajectory tracking performance of the system with the augmented pre-filter P. Trapezoidal velocity reference given by Fig. 5 is used in machine-in-the-loop experiments as well. Fig. 6.b shows convergence performance of the machine-in-the-loop optimization scheme. Iteration "0" corresponds to the case without any pre-filter. Iteration "1" shows the performance with the initial design of the pre-filter  $P_1$  given by Eq. (14). Iterations "2" and "3" show two consecutive iterations where the pre-filter P given by Eq. (15) is used, and filter parameters are updated based on Eq. (18) at each iteration. As seen, convergence is achieved in only two iterations and the maximum tracking error peak is reduced to ~215 [udeq].

## **CONCLUSIONS**

In this paper, we presented an auto-tuning strategy for ultra-precision servo-drives suffering from largely varying load mass inertia. First, a PID controller is tuned based on the experimentally obtained frequency response function of the servo-drive. A safe cross-over frequency for PID tuning is automatically determined based on the modeling accuracy of the open loop system. Stability issues caused by higher order modes induced by large load inertia is prevented by an optimally designed low pass filter. Trajectory tracking bandwidth is expanded by a trajectory pre-filter. Pre-filter parameters are obtained through data-driven machine-in-the-loop iterations.

#### **REFERENCES**

- [1] Varanasi K. K. 2002. On the Design of a Precision Machine for Closed-Loop Performance. PhD Thesis. MIT.
- [2] Erkorkmaz K, Gordon D. J. 2013. Accurate control of ball screw drives using poleplacement vibration damping and a novel trajectory prefilter. Precision Engineering 37(2):308-322.
- [3] Dumanli A, Sencer B. 2018. Optimal high-bandwidth control of ball-screw drives with acceleration and jerk feedback. Precision Engineering 54:254-268.
- [4] Dumanli A, Sencer B. 2019. Precompensation of servo tracking errors through data-based reference trajectory modification. CIRP Annals 68(1):397-400.

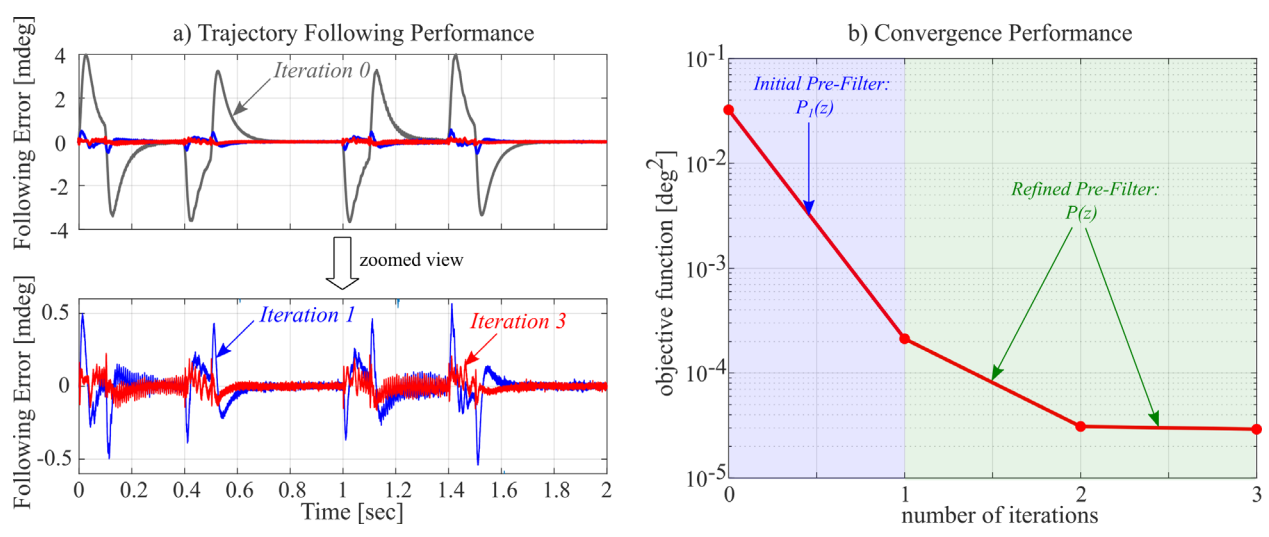


FIGURE 6: Trajectory tracking and convergence performance of the proposed iteratively optimized trajectory pre-filter scheme.